ORNL/TM-6352

The Topology of Tokamak Orbits

James A. Rome
Y.-K. M. Peng

OAK RIDGE NATIONAL LABORATORY
OPERATED BY UNION CARBIDE CORPORATION · FOR THE DEPARTMENT OF ENERGY

ORNL/TM-6352

Dist. Category UC-20 g

Contract No. W-7405-eng-26

FUSION ENERGY DIVISION

THE TOPOLOGY OF TOKAMAK ORBITS

James A. Rome

Y.-K. M. Peng

Date Published: September 1978

Prepared by the

OAK RIDGE NATIONAL LABORATORY

Oak Ridge, Tennessee 37830

operated by

UNION CARBIDE CORPORATION

for the

DEPARTMENT OF ENERGY

TABLE OF CONTENTS

THE TOPOLOGY OF TOKAMAK ORBITS

by James A. Rome and Y.-K. M. Peng

Oak Ridge National Laboratory, Oak Ridge, TN 37830, U.S.A.

ABSTRACT

Guiding center orbits in noncircular axisymmetric tokamak plasmas are studied in the constants of motion (COM) space of (v, ζ, ψ_m). Here, v is the particle speed, ζ is the pitch angle with respect to the parallel equilibrium current $J_{\parallel}$, and ψ_m is the maximum value of the poloidal flux function (increasing from the magnetic axis) along the guiding center orbit. Two D-shaped equilibria in a flux-conserving tokamak having β's of 1.3% and 7.7% are used as examples. In this space, each confined orbit corresponds to one and only one point and different types of orbits (e.g. circulating, trapped, stagnation and pinch orbits) are represented by separate regions or surfaces in the space. It is also shown that the existence of an absolute minimum B in the higher β (7.7%) equilibrium results in a dramatically different orbit topology from that of the lower β case. The differences indicate the confinement of additional high energy ($v \rightarrow c$, within the guiding center approximation) trapped, co- and countercirculating particles whose orbit ψ_m falls within the absolute B well.

I. INTRODUCTION

Fast ions with large banana widths are becoming increasingly common in tokamaks as a result of neutral beam injection, alpha particle production, and radio frequency heating . To treat these fast particles properly, it is essential that their guiding center orbits be accurately known. For example, the particle orbit loss region[1] and alpha particle wall loading calculations[2] rely entirely on large banana width effects.

Many of the usual "small banana width" approximations are misleading or wrong when applied to large banana width particles. An instance of this is the assumption that particles with a pitch angle of 90° are deeply trapped; in fact, such particles are on the boundary of the trapping region.

Our main aim in this work is to bring logic and order to bear on the task of describing, classifying, and understanding the plethora of possible tokamak orbits. Furthermore, this must be done for the noncircular, high β equilibria that are of interest in many new tokamaks. It is not enough to know what an orbit looks like; we must also know its generic type and its collisional transition to other types of orbit. We propose to do this by classifying the guiding center orbits in the three-dimensional constants of motion (COM) space that completely characterize such orbits in axisymmetric tokamaks.

A practical reason for elucidating this orbit topology is to enable the bounce-averaged Fokker-Planck equation[1] to be set up and solved in the COM space. Since each point in this space represents an entire bounce orbit, and collisions of fast ions occur slowly compared

BLANK PAGE

to a bounce time, the time step needed to perform numerical calculations in this space is determined by the collision time rather than the bounce time. Knowledge of the fast ion distribution function in the COM space allows computation of macroscopic quantities which change slowly compared to a bounce time.

In the remainder of this paper, we will discuss the choice of a set of constants of motion, make such a choice, and examine the orbit topology in this space. The results will be presented graphically in the COM space.

II. PICKING THE CONSTANTS OF MOTION

Three constants of motion are needed to completely characterize the guiding center motion of a particle in an axisymmetric tokamak. Usually, the three COM are taken to be ε (the energy), μ (the magnetic moment), and p_ϕ (the toroidal canonical angular momentum), but this set is inconvenient for the present task, and a better choice can be made.

To decide what constitutes a "good" set of COM, we can invoke some guidelines. First, the coordinates should be <u>physically meaningful</u> with easily calculated values. p_ϕ is inconvenient in this respect since it mixes configuration space and velocity space. The coordinates should (if possible) be <u>orthogonal</u> to eliminate cross-derivatives in the Fokker-Planck equation. Thus, Cartesian or polar coordinates in velocity space are preferable to ε and μ.

It is important to pick a representation that is unique; i.e., a given point in the COM space should correspond to one and only one particle orbit and vice versa. The conventional COM set, (ε , μ , p_ϕ), does not satisfy this requirement due to the indeterminancy of the sign of $v_\parallel$ in p_ϕ. For instance, in the usual zero banana width limit the trapped particles are represented twice, once for each sign of $v_\parallel$.

Finally, we wish our space to be well filled. By this we mean that a valid orbit should result from most choices of the three COM; it should be contained in the tokamak and not defined elsewhere in the space. In this respect, ε , μ , p_ϕ space proves to be mostly empty and multisheeted.

Of course, it should be noted that the topology has the same features no matter how it is represented. But the result will be easier to use and comprehend if we make a "good" choice of the COM.

At this point, we will simplify our task by placing some restrictions on the flux surface geometry. In the cylindrical R, ϕ, z coordinate system with the symmetry axis corresponding to that of the tokamak, we require that the poloidal flux function, $\psi(R,z)$, be symmetric in z and monotonic for $z > 0$. Also, there must be only one magnetic axis. Thus, the only configuration of practical interest that we rule out is the Doublet. Due to our assumed symmetry, we will only consider orbits for $z \geq 0$ in this paper.

Generally, we will consider equilibria obtained from the solution of the Grad-Shafranov equation, especially those resulting in high values of β (the ratio of plasma pressure to magnetic field pressure) such as in the flux-conserving tokamak.[3] However, recent work by Northrop and Rome[4] has shown that for high β ($\gtrsim 10\%$), the orbits derived

using the COM approach differ significantly from those derived from the guiding center equations of motion. Although this difference is of second order in gyroradius, it is not negligible in the high β case. Since the guiding center equations are valid to all orders and the usual COM are not, the COM approach should only be used for $\beta \lesssim 10\%$.

Since tokamak orbits may be regarded as a competition between motion along a field line and the $\overline{B} \times \nabla B$ and curvature drifts, the particle orbit will be a monotonic function of ψ in the top half of the torus. The two orbit crossings of the equatorial plane must occur at the maximum (ψ_m) and minimum (ψ_n) values of ψ. Because of these properties, ψ makes a convenient variable with which to denote a position along the orbit ($\psi_n \leq \psi \leq \psi_m$). ψ_m is then a good choice for a constant of the motion because if $\psi_m > \psi_{wall}$, the particle is in the loss region. In accord with previous fast ion treatments,[1] we pick the velocity space coordinates v, the speed, and $\zeta = (\overline{v}\cdot\overline{J}_{\parallel})/(vJ_{\parallel})_{\psi_m}$, the cosine of the angle between the particle velocity and $J_{\parallel}$. We use the sign of $\overline{v}\cdot\overline{J}_{\parallel}$ and not $\overline{v}\cdot\overline{B}$ because the orbit trajectory is independent of the sign of the latter quantity. If $\overline{v}\cdot\overline{J}_{\parallel} > 0$, (< 0), the particle is "co" ("counter").

Thus, the three constants of motion are (v, ζ, ψ_m). Our task is to examine the nature of the particle orbits at any point in this space.

III. GUIDING CENTER ORBITS

Because the topological features of the COM space are most easily seen at high energies, we will treat the guiding center orbits relativistically. Even though the guiding center approximation breaks down as the energy is increased, we need to know the topology at very high energies in order to understand it at the lower energies of interest.

Through first order in gyroradius, the toroidal canonical angular momentum of the guiding center is conserved:[4]

$$p_\phi = \gamma m R v_\phi - Ze\psi = \text{constant}. \tag{1}$$

Z is the charge number of the ion, $\gamma = [1 - (v/c)^2]^{-1/2}$, R is the distance from the z axis to the guiding center, and mks units are used throughout the paper. For the guiding center, $v_\phi = v_\parallel B_\phi/B$ and we have defined ψ so that it is zero at the magnetic axis and has the (positive) value ψ_{wall} at the plasma chamber.

For ideal MHD equilibria, RB_ϕ is only a function of ψ :

$$RB_\phi = F(\psi). \tag{2}$$

In terms of our constants of motion, we may write the parallel velocity at any point along the orbit as

$$v_\parallel = \pm v\sqrt{1 - (1 - \zeta^2)\frac{B}{B_m}} \quad . \tag{3}$$

where the subscript m indicates values at $\psi = \psi_m$ along the orbit.

Using Eqs. 2 and 3, and evaluating Eq. 1 at ψ_m and at a general point along the orbit, yields the orbit equation for $B(\psi)$:

$$B = \frac{B_m}{(\frac{1-\zeta^2}{2}) + \{(\frac{1-\zeta^2}{2})^2 + (\frac{F_m}{F})^2 [\zeta - G_m(1 - \frac{\psi}{\psi_m})\sqrt{\frac{c^2}{v^2} - 1}\ ]^2\}^{1/2}} , \tag{4}$$

where the dimensionless parameter G_m is defined by

$$G_m = \frac{ZeB_m\psi_m}{mcF_m} . \tag{5}$$

Since the B = constant and ψ = constant surfaces are nonparallel for β's of interest, we can regard them as a (nonorthogonal) coordinate system in which to plot the ion orbits. In Fig. 1, we employed an MHD equilibrium code[5] to obtain the flux surfaces (dotted) and B contours for $\beta = 1.3\%$ and $\beta = 7.7\%$. At low β, the B contours are almost vertical but as β increases, a striking change takes place. A local minimum in B forms between the magnetic axis and the outside edge of the plasma. It is this change that will be responsible for the changes in the orbit topology at high β.

It is appropriate to comment upon this natural choice of B and ψ as variables to use for plotting the orbits. From Eq. 4, we see that we can explicitly solve for $B(\psi)$ along an orbit for a given equilibrium with no approximations. This situation manifests itself in many of the formulas of neoclassical theory in which B and ψ appear.

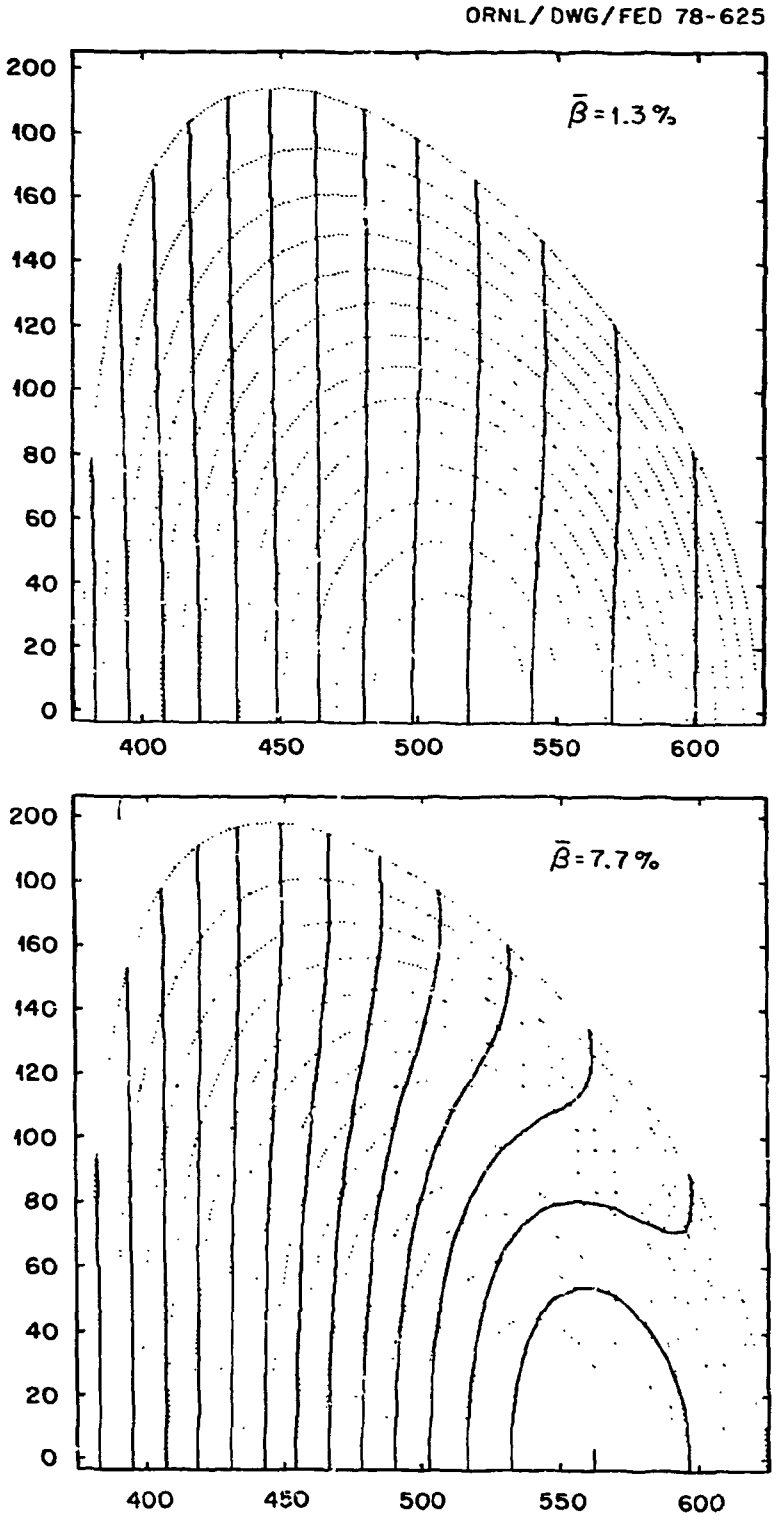

FIGURE 1. Flux surfaces (dotted) and mod B contours for β = 1.3% and 7.7% in a prototypical power reactor.

In accord with this, we can regard B and ψ as our fundamental coordinates and invert the Grad-Shafranov equation to find R and z as functions of B and ψ.

Using the results of Fig. 1, we can take the values of B along the equatorial plane and plot them versus ψ (normalized to their values at the inside wall). This curve is denoted by $(B\text{-}\psi)_{eq}$ in Fig. 2. Since the particle orbits move monotonically in ψ, they will intersect the $(B\text{-}\psi)_{eq}$ curve twice, at ψ_n and ψ_m and their trajectories will lie in the region shown in Fig. 2. Depending upon the orbit, these intersections may occur inside or outside the magnetic axis.

This can be pinned down more precisely by differentiating Eq. 4 with respect to $\psi/\ \psi_m$ (denoted by a prime) and evaluating the result when $\psi = \psi_m$:

$$\frac{B'_m}{B_m} = \frac{2\zeta}{1+\zeta^2}\left(\frac{F'_m}{F_m}\zeta - G_m\sqrt{\frac{c^2}{v^2}-1}\right) \quad . \tag{6}$$

For a valid orbit, the particle must start off at ψ_m and go to smaller values of ψ. A limit on the starting slope of the orbit in $B\text{-}\psi$ space occurs when the orbit is tangent to the $(B\text{-}\psi)_{eq}$ curve. If B_{in} is the magnitude of B on the equator inside the magnetic axis, and B_{out} is the magnitude outside the magnetic axis,

$$\left.\frac{B'_m}{B_m}\right|_{in} < \frac{2\zeta}{1+\zeta^2}\left(\frac{F'_m}{F_m}\zeta - G_m\sqrt{\frac{c^2}{v^2}-1}\right) \quad \text{FOR } \psi_m \text{ INSIDE MAGNETIC AXIS,} \tag{7}$$

$$\left.\frac{B'_m}{B_m}\right|_{out} > \frac{2\zeta}{1+\zeta^2}\left(\frac{F'_m}{F_m}\zeta - G_m\sqrt{\frac{c^2}{v^2}-1}\right) \quad \text{FOR } \psi_m \text{ OUTSIDE MAGNETIC AXIS.}$$

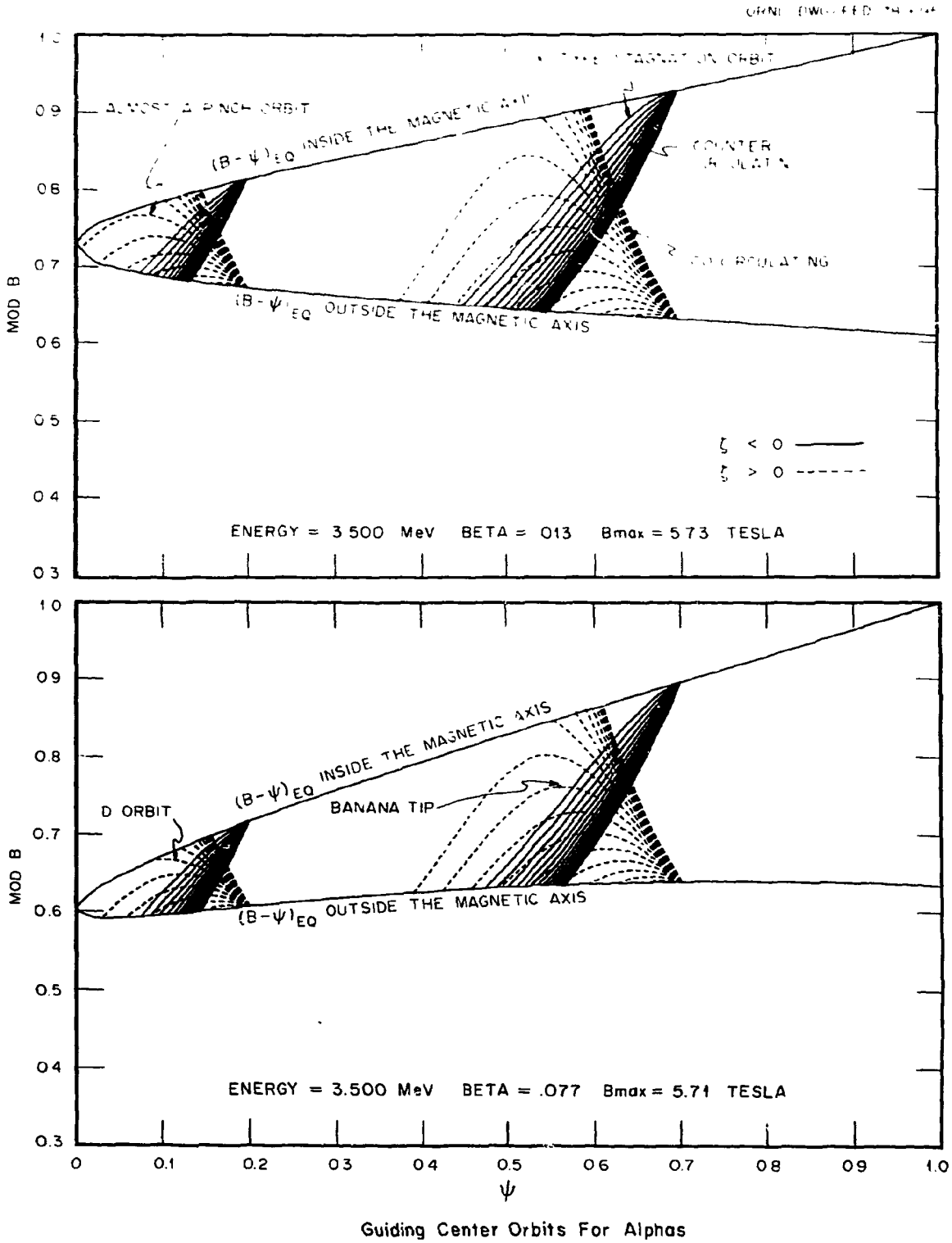

FIGURE 2. Alpha particle orbits in B-ψ space for three values of ψ_m and various values of ζ. Orbits with $\zeta < 0$ are dashed. The orbits are bounded by the $(B-\psi)_{eq}$ curve.

For high β equilibria, $B'_{in} > 0$, B'_{out} may have either sign, and if $\beta_{poloidal} \geq 1$, $F' > 0$. Under these conditions, orbits with ψ_m inside the magnetic axis will have $\zeta < 0$; orbits with ψ_m outside the magnetic axis will have $\zeta > 0$ and may also have $\zeta < 0$ if $B'_{out} > 0$.

This situation is made clearer in Fig. 2 which shows various alpha particle orbits in a prototypical reactor for three values of ψ_m and for various values of ζ, according to Eq. 4 . Orbits with $\zeta > 0$ are shown dashed. The detailed features of the various types of orbits will be pointed out later in the paper. For now, we note that circulating ions move monotonically in B whereas trapped ions have a maximum in B along the orbit at the mirror point (the banana tip). Co-going ions have a negative value of B' while countergoing ions have a positive B' along the orbit. In Fig. 3, we show the correspondence of orbits in B-ψ space to orbits in configuration space. The most important orbit quantity, its deviation from a flux surface is readily obtained in either space.

Representation of the orbits in B-ψ space is straightforward and often yields more insight into the orbit topology. Consequently, for studying orbits or for solving problems in the COM space, our strategy will be to do as many calculations as possible in the COM space or B-ψ space,and only go to configuration space when necessary or to make contact with the traditional body of knowledge.

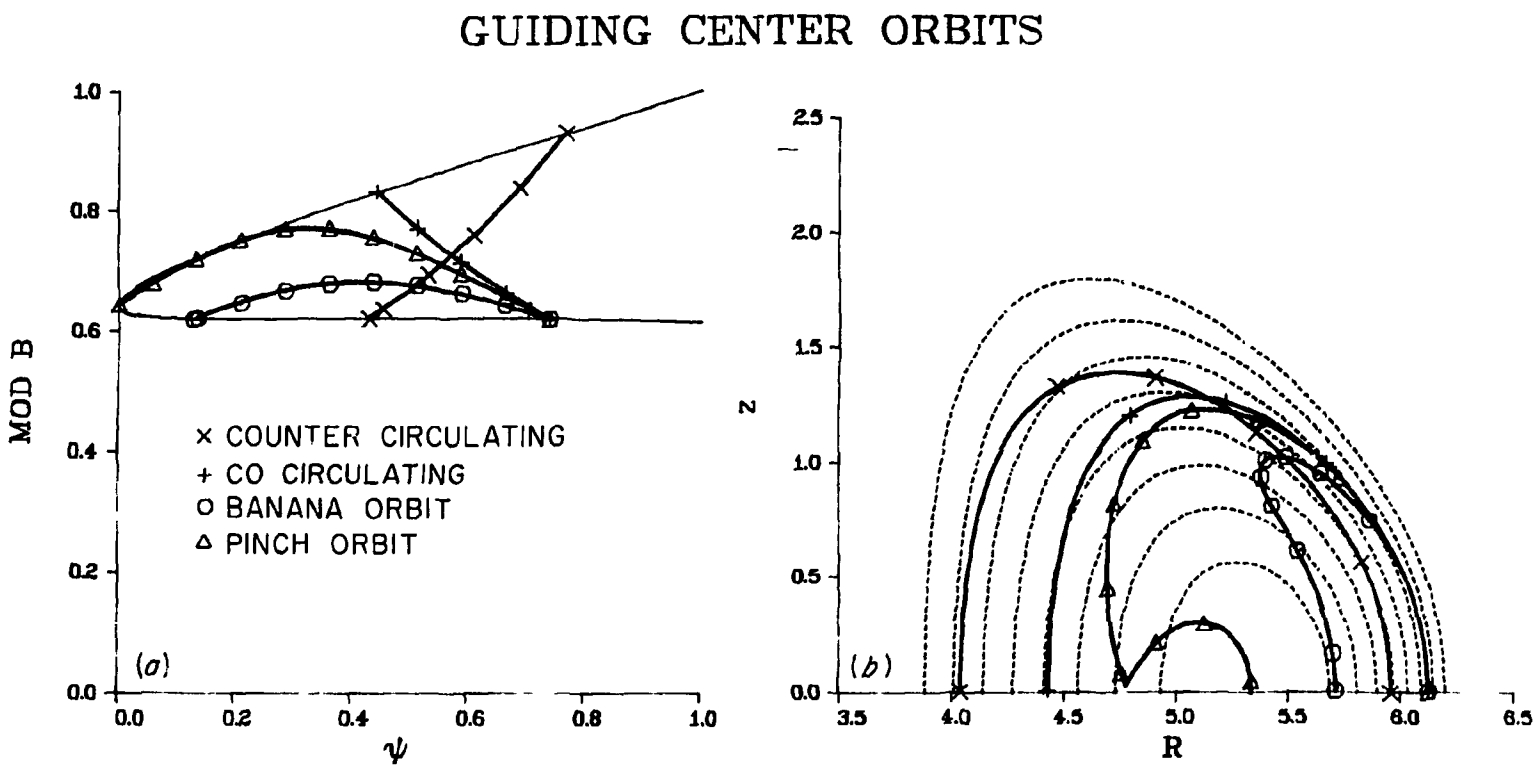

FIGURE 3. The correspondence between orbits in (a) B-ψ space and (b) configuration space.

IV. THE TRAPPED PARTICLE REGION

A trapped particle is one for which $v_{\parallel} = 0$ somewhere along the orbit. By topologically deforming a banana orbit, we can see that there are two ways in which an orbit could have become trapped. If the banana orbit deforms so that it becomes kidney-shaped and then D-shaped, the tips will approach the equator and merge there; $v_{\parallel}$ will be zero on the equator. Alternatively, the orbit may deform while maintaining its banana shape so that the points of the banana "pinch" on the equator if $v_z = 0$ there. These D orbits and pinch orbits are illustrated in Fig. 4.

First we consider the locus of D orbits in v, ζ, ψ_m space. From the p_ϕ equation (Eq. 1), we see that the $v_{\parallel} < 0$ part of banana orbits must occur at smaller values of ψ than the $v_{\parallel} > 0$ part of the orbits. Thus, for D orbits, the banana tip must occur at either ψ_m or ψ_n. The former situation can only occur in the high β case outside the magnetic axis in the region where B' is positive. Otherwise, from Eq. 3 we see that the tip occurs at

$$B_n = \frac{B_m}{1 - \zeta^2}. \tag{8}$$

Accordingly, Eq. 4 can be solved for v/c at the banana tip:

$$\frac{v}{c} = \left[1 + \left(\frac{\zeta}{G_m(1 - \psi_n/\psi_m)}\right)^2\right]^{-1/2}. \tag{9}$$

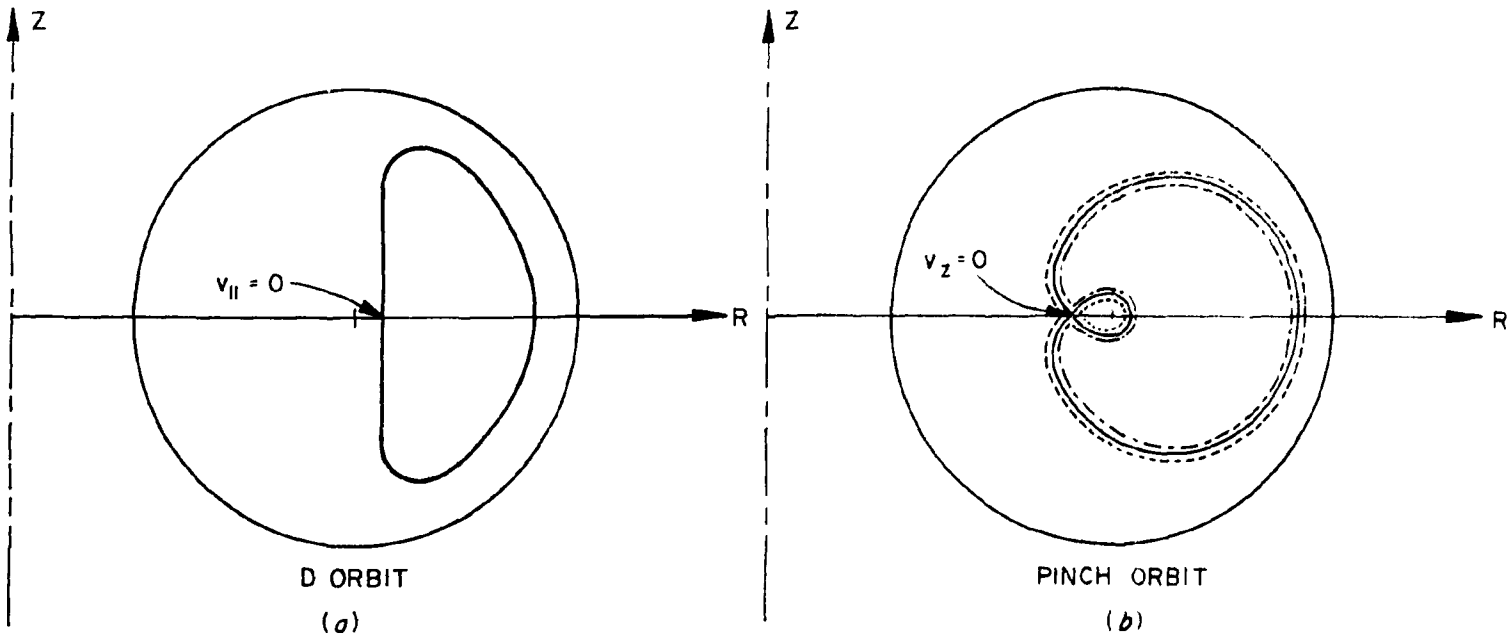

FIGURE 4. The two types of "barely trapped" orbits. (a) A D orbit which has $v_{||} = 0$ on the equator. (b) A pinch orbit which has $v_z = 0$ on the equator at the pinch point.

Equations 8 and 9 must be used together with the $(B\text{-}\psi)_{eq}$ curve to determine the trapping region locus as shown in Fig. 5. To do this, we pick a value of ψ_m and find its corresponding B_m. The lower value of B_m must be used to insure that $\psi_m > \psi_n$. Additionally, for $\zeta > 0$, ψ_m occurs outside the magnetic axis. We divide this by $1 - \zeta^2$ to find B_n and its corresponding ψ_n. Then Eq. 9 yields the value of v/c for the chosen values of ζ, ψ_m.

Plots of the resulting locus of D orbits (which is the trapping region boundary) are shown in Fig. 6 for the low and high β cases. Particles under the plotted surfaces are trapped. Several observations of interest can be made here. First, trapped particles only occur for $\zeta > 0$. This is because we define our trapped particles at only one point in the COM space and all banana orbits have their maximun value of ψ on the $v_{\parallel} > 0$ half of the orbit. Next, for the low β case, there is a definite energy above which no trapped particles exist, in accord with the work of McAlees.[6] This is due to the fact that the drifts ($\sim v^2$) completely dominate the poloidal component of motion along a field line ($\sim v$). This situation can occur at low energies near the magnetic axis since $B_{poloidal}$ approaches zero.

Finally we note that the zero banana width concept of a "very trapped" particle needs readjustment. These particles are usually taken to have a pitch angle of 90° on the equatorial plane. As we have seen, such particles are in fact at the edge of the trapping region! This difference is due to the three-dimensional nature of the magnetic mirror. If we plot B along a field line and put a particle at the bottom of the well (which occurs on the equator) with no $v_{\parallel}$, it would appear that the particle is deeply trapped. But all the particle must

ORNL/DWG/FED 78-628

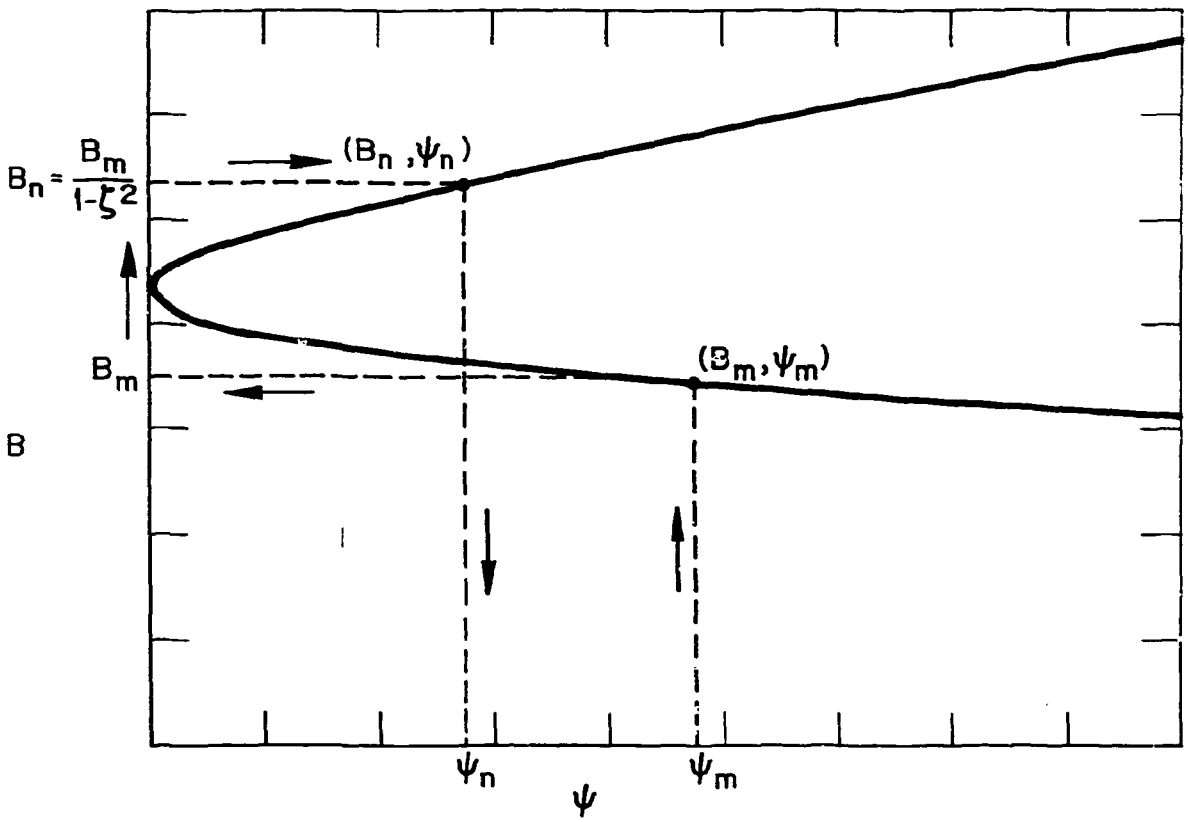

FIGURE 5. The procedure for using the $(B\text{-}\psi)_{eq}$ curve to find the locus of D orbits.

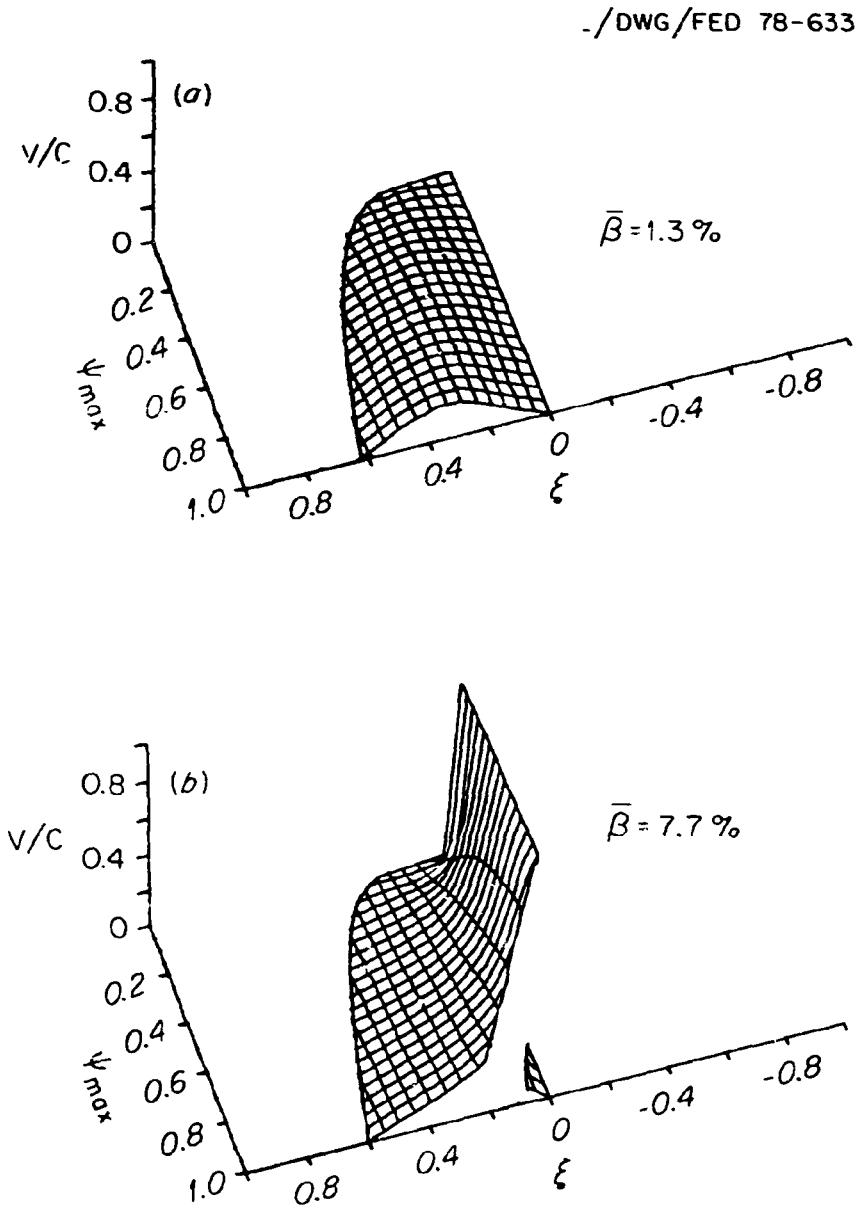

FIGURE 6. The trapping region boundary. (a) β = 1.3%. (b) β = 7.7%.

do to gain some $v_{\parallel}$ is to move outward in major radius to a region of lower B. It will then execute a D orbit. Such motion is unallowed in the zero banana width limit but must occur if the banana width has any finite value. If the particle were to start at the same location with an infinitesimal value of $v_{\parallel}$ (and a concomitant value of ζ just outside the trapping region), it would be a circulating particle, continuously encircling the z axis.

For the high β case (Fig. 6b), particles can be trapped at any energy in the region where $B'_{out} > 0$. Also, the boundary of the trapping region is composed of two separate parts. Both of these effects are due to the minimum in B. In the region where $B' > 0$, the banana tip can be located at ψ_m, and the orbit must go "downhill" from there. Thus, as the particle energy is increased, the orbit only becomes more horizontal. As ψ_m moves outward past the maximum in B (a saddle point in the B contours), the tip may no longer occur at ψ_m, and the topology changes back to that of the low β case.

The locus of pinch orbits will be found to lie within the trapped particle region of Fig. 6. Because the physics of the pinch orbit is quite different and specialized, we will consider it separately in a later section. In conclusion, all trapped particles have $\zeta > 0$ and lie within the region of v, ζ, ψ_m space which is shown in Fig. 6. For sufficiently high energy, there are no trapped particles in the low β case.

V. STAGNATION ORBITS

All of the other features of the COM space may be regarded as singularities. These singular orbits have the property that they remain fixed at one poloidal location in the absence of collisions. This location is called a stagnation point and the orbit is called a stagnation orbit. Of course, a particle on this type of orbit will still move toroidally because $v_{\parallel}$ cannot be zero at a stagnation point.

There are two types of stagnation points that may be regarded as being either stable or unstable and correspond to the O-points or X-points which often appear in topology studies. In the former case, a small displacement leaves the particle in the vicinity of the O-point while in the latter, a small displacement will cause a large excursion away from the X-point.

The occurrence of a stagnation point is caused by the cancellation of the vertical motion due to following a field line with that due to the $\bar{B} \times \nabla B$ and curvature drifts. This circumstance can only happen in the equatorial plane where both of these motions are purely vertical by symmetry. While we could derive the conditions for these orbits by setting the vertical component of the equation of motion to zero, it is more appropriate to do so from the p_ϕ equation. Since the curves p_ϕ = constant represent orbits, it is easy to see that the stagnation points must occur when $dp_\phi/dR = 0$ on the equator,[4]

$$\frac{1}{e}\frac{dp_\phi}{dR} = \gamma\frac{m}{e}\left[v_\parallel \frac{d}{dR}\left(R\frac{B_\phi}{B}\right) - \frac{\mu B_\phi R}{mB\,v_\parallel}\frac{dB}{dR}\right] - \frac{d\psi}{dR} = 0 \quad . \tag{10}$$

We can use the chain rule to express all derivatives with respect to ψ, and make use of the relation $d\psi/dR = \pm RB_z$ on the equator (the + sign is for $R > R_0$, the magnetic axis location).

By substituting for $v_{\parallel}$ we can solve for $\gamma v/c$:

$$\gamma \frac{v}{c} = \frac{\pm G_m \sqrt{1 - (1 - \zeta^2)\frac{B}{B_m}}}{[1 - (1 - \zeta^2)\frac{B}{B_m}](\frac{FB_m}{BF_m})' - \frac{1}{2}(1 - \zeta^2)\frac{F B'}{F_m B}} . \qquad (11)$$

Only positive solutions for v/c are physically acceptable. For the case of an orbit with a stagnation point at $\psi = \psi_m$, this condition simplifies to

$$\gamma \frac{v}{c} = \frac{G_m \zeta}{\zeta^2 \frac{F'_m}{F_m} - \frac{1}{2}(1 + \zeta^2)\frac{B'_m}{B_m}} . \qquad (12)$$

These same conditions can be derived by noticing with the aid of Fig. 2 and Eq. 6 that the stagnation orbits must occur when $dB/d\psi$ along the orbit = $dB/d\psi$ along the equator, i.e., the orbit trajectory comes off at a tangent to the $(B\text{-}\psi)_{eq}$ curve of Fig. 2.

The surface represented by this equation is the desired locus of the O-type stagnation orbits and some of the X-type stagnation orbits. In Fig. 7 we show the stagnation orbit locus for stagnation points occurring inside the magnetic axis for both values of β. The three regions of these surfaces will be discussed later. In Fig. 8 we show similar surfaces for stagnation points occurring outside the magnetic axis. In this case, there is a drastic change in topology in the

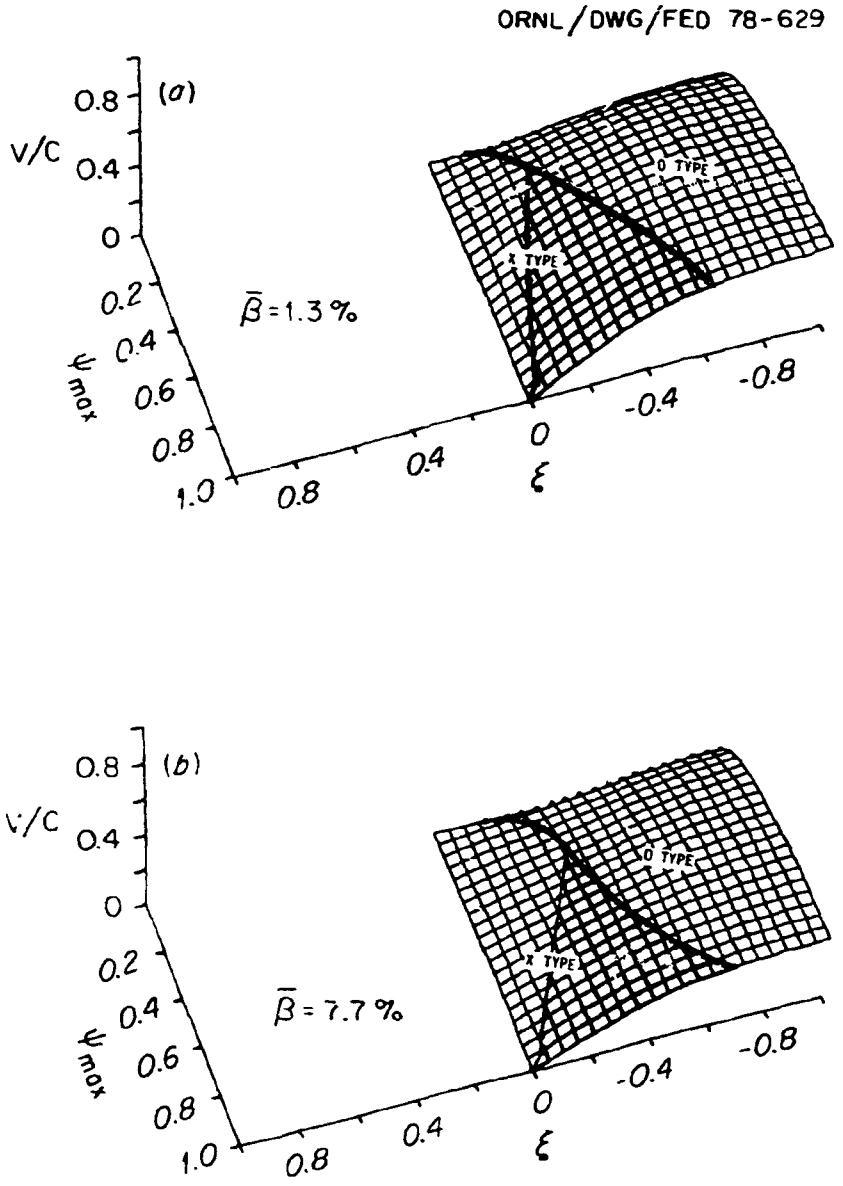

STAGNATION ORBITS WITH ψ_m INSIDE THE MAGNETIC AXIS (THE LOSS REGION IS IN BOLD LINES)

FIGURE 7. The stagnation orbit locus for orbits with stagnation points occurring at ψ_m inside the magnetic axis. The loss region is shown in bold lines. (a) β = 1.3%. (b) β = 7.7%.

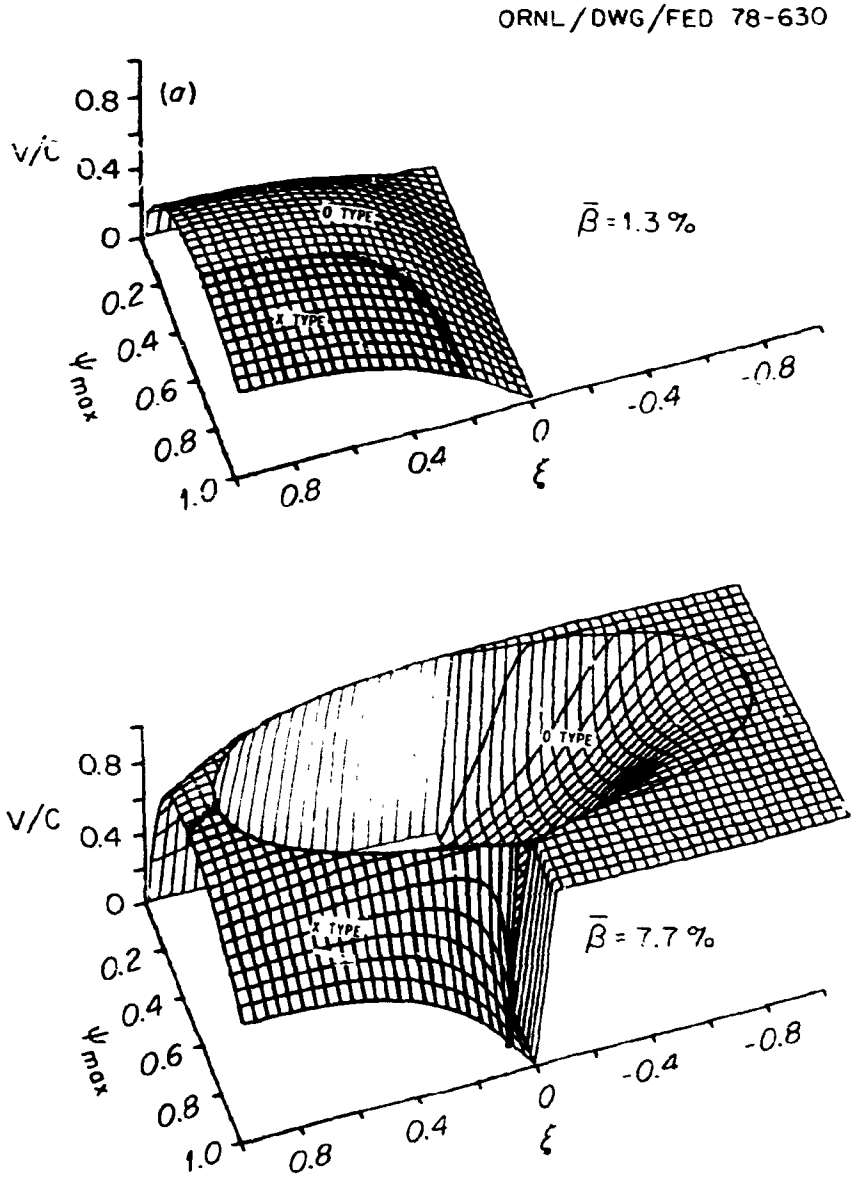

FIGURE 8. The stagnation orbit locus for orbits with stagnation points occurring at ψ_m outside the magnetic axis. The loss region is shown in bold lines. (a) β = 1.3%. (b) β = 7.7%.

region where $B'_m > 0$. In this region, the stagnation orbit locus extends up to v/c = 1 and some orbits are allowed for $\zeta < 0$.

Except for the $\zeta < 0$ region of Fig. 8b, the region of COM space above the surfaces of Figs. 6 and 7 represents a forbidden region of the COM space. The reason for this is that the mathematics describing the orbits would work just as well if we had picked ψ_n as our third constant of motion instead of ψ_m. Orbits in the forbidden region have ζ defined at ψ_n instead of ψ_m and if these orbits are contained in the tokamak they will be defined elsewhere in the COM space. Thus, the forbidden region serves to maintain the single-valuedness of our representation.

For example, suppose we consider an orbit in the forbidden region with $\zeta = 0$ at some $\psi_m \neq 0$ and at a smallish value of v. Since $v_{\shortparallel} = 0$, the orbit will drift vertically until the rotational transform pulls the particle radially outward and along the flux surface. The orbit will be a D orbit (Fig. 4) and it will have a ψ_m greater than the one we had originally picked (which turned out to be ψ_n). ζ will not be zero for this orbit since $v_{\shortparallel} \neq 0$ at the definition point, ψ_m.

In the high β case, for $\zeta < 0$, the forbidden region lies between the surfaces of Figures 6b and 7b. The region of valid orbits with ψ_m outside the magnetic axis for $\zeta < 0$ leads to a new type of orbit not present at low β. These orbits are countercirculating orbits which stay close to the equatorial plane outside of the magnetic axis.

Notice that the two regions of valid orbits are entirely separated and that so far, there is no mechanism whereby a particle can scatter from one region of valid orbits to the other region. As it must, the trapped particle region lies entirely within the region of acceptable

orbits and for high β, the two separate regions of the trapping boundary are joined by the stagnation orbit locus.

VI. THE TRANSITION FROM X-TYPE ORBITS TO O-TYPE ORBITS

Some of the stagnation orbits with their stagnation point at ψ_m are X-type and some are O-type. Since Eq. 12 describes both X- and O-type stagnation orbits, it is important to know when the transition between the two orbit types occurs. Physically, this takes place when the X-type orbit shrinks in size, i.e. when $\psi \rightarrow \psi_m$. In this limit, we can expand the orbit equation (Eq. 4) in ψ about ψ_m and solve for ψ_n under the condition that Eq. 12 holds. The result of doing this is that

$$B''_{\text{along orbit at } \psi_m} = B''_{\text{along equator at } \psi_m} \quad . \tag{13}$$

This result can also be seen by looking at the B-ψ representation of the orbit: X-type stagnation orbits leave tangent to the $(B\text{-}\psi)_{eq}$ curve and the orbit size will shrink to zero as Eq. 13 becomes satisfied. Taking the second derivative of Eq. 4 and substituting it into Eq. 13 yields a biquadratic equation for ζ:

$$\zeta^4\{4F''_m - 4B'_mF'_m - 2B''_m + 3(B'_m)^2\}$$

$$+ \zeta^2\{6(B'_m)^2 - 2B''_m - 4B'_mF'_m\} - (B'_m)^2 = 0 \quad . \tag{14}$$

Numerically, this equation presents evaluation difficulties due to the second derivatives of the equilibrium quantities. To overcome these, the equilibria had to be calculated on a very fine mesh and then fitted with a spline.

Of course since Eq. 12 must hold, the above locus must lie on the forbidden region boundaries of Figs. 6 and 7. As can be seen in the figures, the X-type stagnation orbits only occur at low energies for $\zeta < 0$. The X-type orbits with $\zeta > 0$ can only occur near the outside of the plasma in the region where $B_{poloidal}$ is a decreasing function of ψ.

VII. THE PINCH ORBITS AND LOSS REGIONS

There is one last type of stagnation orbit to be dealt with, the pinch orbit. The pinch orbit is the only orbit for which the stagnation point does not occur at ψ_m, and it is in some sense the "fattest" of all banana orbits.[7]

Since the pinch orbit is the most topologically complex orbit, it deserves careful consideration. There are two types of pinch orbits, as illustrated in Fig. 9, according to whether the pinch point lies inside or outside the magnetic axis. The former type of orbit is called a "copinch" orbit while the latter is called a "counterpinch" orbit. As shown in Fig. 9, there are three adjacent orbits onto which

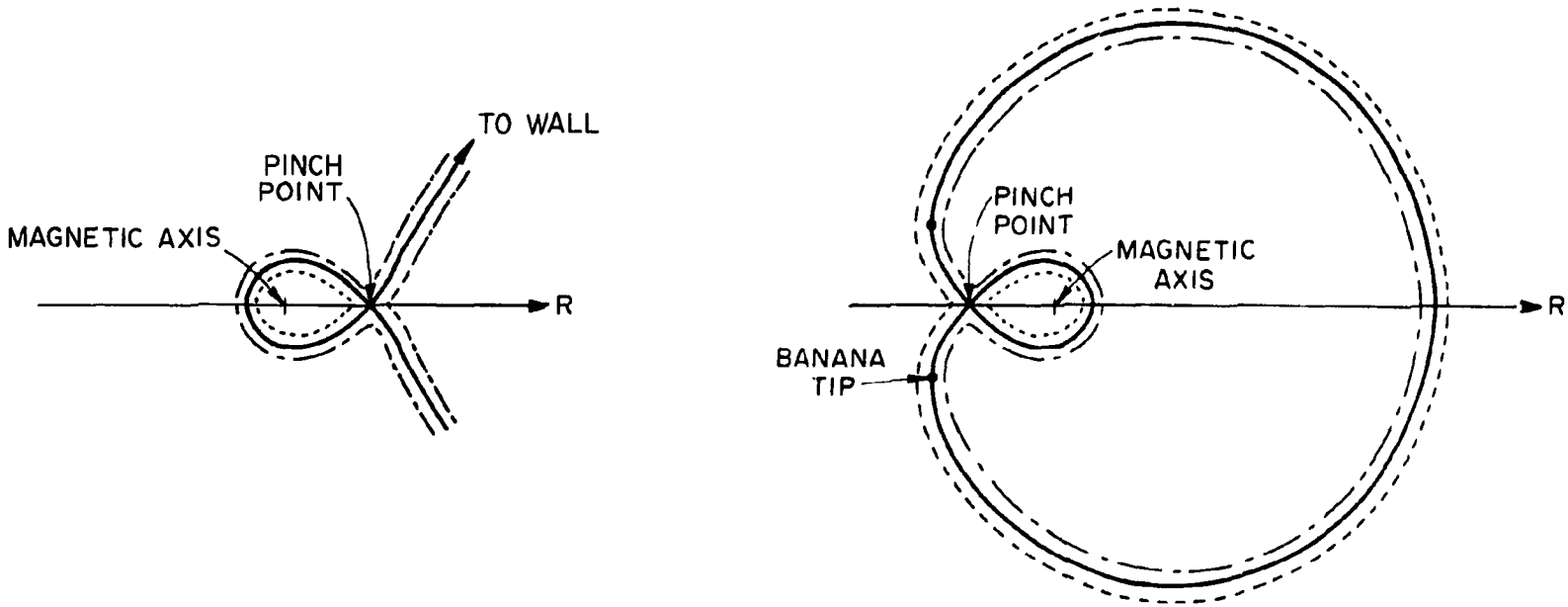

FIGURE 9. The two types of pinch orbits together with the neighboring orbits onto which they may scatter. (a) The copinch orbit with the pinch point occurring with $v_{\|} > 0$. (b) The counterpinch orbit with the pinch point occurring with $v_{\|} < 0$.

a particle on a pinch orbit may scatter. The innermost of these orbits is always an X-type stagnation orbit as discussed in Sect. VI.

In the case of the copinch orbits, ψ_m is always outside the plasma since these orbits would have appeared elsewhere in our topology if ψ_m were inside the plasma. Thus, the copinch orbit is always in the loss region. Because the "co" X-type stagnation orbit is the only contained orbit which borders the copinch orbit, the entire X-type stagnation point locus with $\zeta > 0$ is the boundary of the loss region as shown in Fig. 8.

However, for injection and alpha particle studies, the counterpinch orbit is of more practical interest. From Fig. 9 we can see that a particle on a "counter" X-type stagnation orbit (....) with $\zeta < 0$ can scatter onto the enclosed (-.-.) banana orbit, which can then scatter onto the outermost (----) kidney orbit. Since the latter two orbits have $\zeta > 0$, the pinch orbit serves as the only vehicle for connecting the two halves of the orbit topography.

To directly solve for the counterpinch orbit locus, we can solve for v/c in the orbit equation (Eq. 4) and set it equal to the right-hand side of Eq. 11 with all functions of ψ evaluated at the pinch point (subscript p). The resulting equation is a quadratic in w where

$$w = 1 - (1 - \zeta^2)\frac{B_p}{B_m} \quad : \tag{15}$$

$$w^2\{-4B_mB_p{}^3F_m{}^2+B_m{}^2[(\psi_m-\psi_p)(2B_pF'_p-F_pB'_p)+2B_pF_p]^2\}$$

$$+w\{-4(B_p-B_m)B_p{}^3F_m{}^2-2B_m{}^2B'_pF_p(\psi_m-\psi_p)[(\psi_m-\psi_p)(2B_pF'_p-F_pB'_p)+2B_pF_p]\}$$

$$+\{B_mB'_pF_p(\psi_m-\psi_p)\}^2 = 0 \quad . \tag{16}$$

Equation 16 is still implicit. To use it, one chooses a value of ψ_m and then steps through all values of $\psi_p < \psi_m$. For each pair (ψ_m, ψ_p), we find w from Eq. 16 and ζ from Eq. 15. The value of v/c is then obtained from Eq. 11.

While doing the above process, the value of v/c for the pinch orbit will increase. A limit will occur when both the first and second derivatives of the orbit equation match those of the $(B-\psi)_{eq}$ curve at the pinch point. This condition is shown in B-ψ space in Fig. 10 and the locus of these orbits corresponds to the O-type to X-type transition of Eq. 14 mapped onto ψ_m (instead of ψ_p) via Eq. 4. Thus, the pinch orbit locus is fully determined and is plotted in Fig. 11.

As we expected from the orbit picture in Fig. 9, the pinch orbit locus must lie just inside the trapping boundary (compare to Fig. 5). The outermost kidney orbit, which is almost a D orbit, lies in the narrow region between the pinch locus and the trapping region boundary. The inner banana orbit lies just on the other side of the pinch orbit locus. A circulating "co" particle can become barely trapped and scatter through the kidney-shaped orbits to the pinch orbit locus. At that point, it can either go through this locus and become a banana orbit, or it can "fall into" the pinch orbit and become a countercirculating orbit at a smaller value of ψ_m. The probability of going either way may be determined by the ratio of the bounce times on the contiguous pieces of the three pinch orbits.

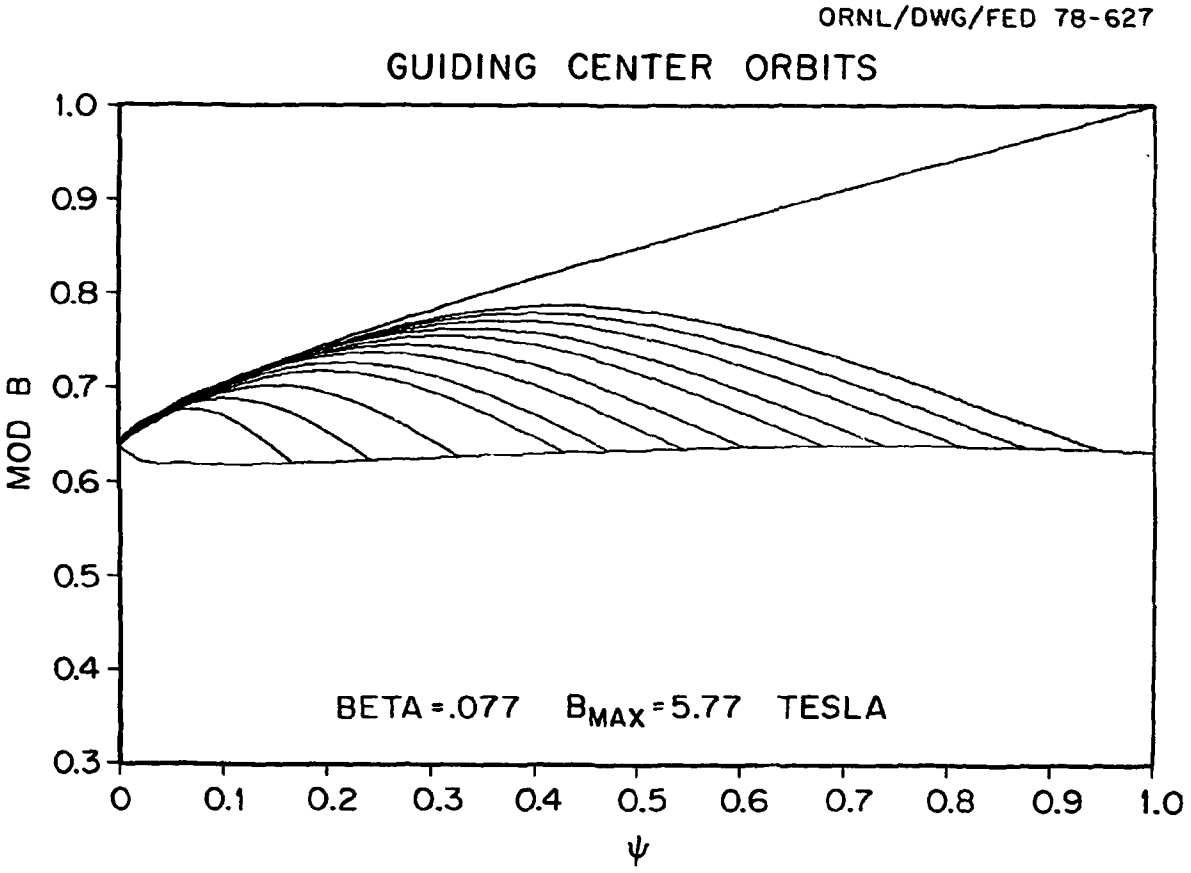

FIGURE 10. The end of the pinch orbit locus occurs when B′ and B′′ along the orbit both match B′ and B′′ along the equator at the pinch point. The last pinch orbits are shown in B-ψ space.

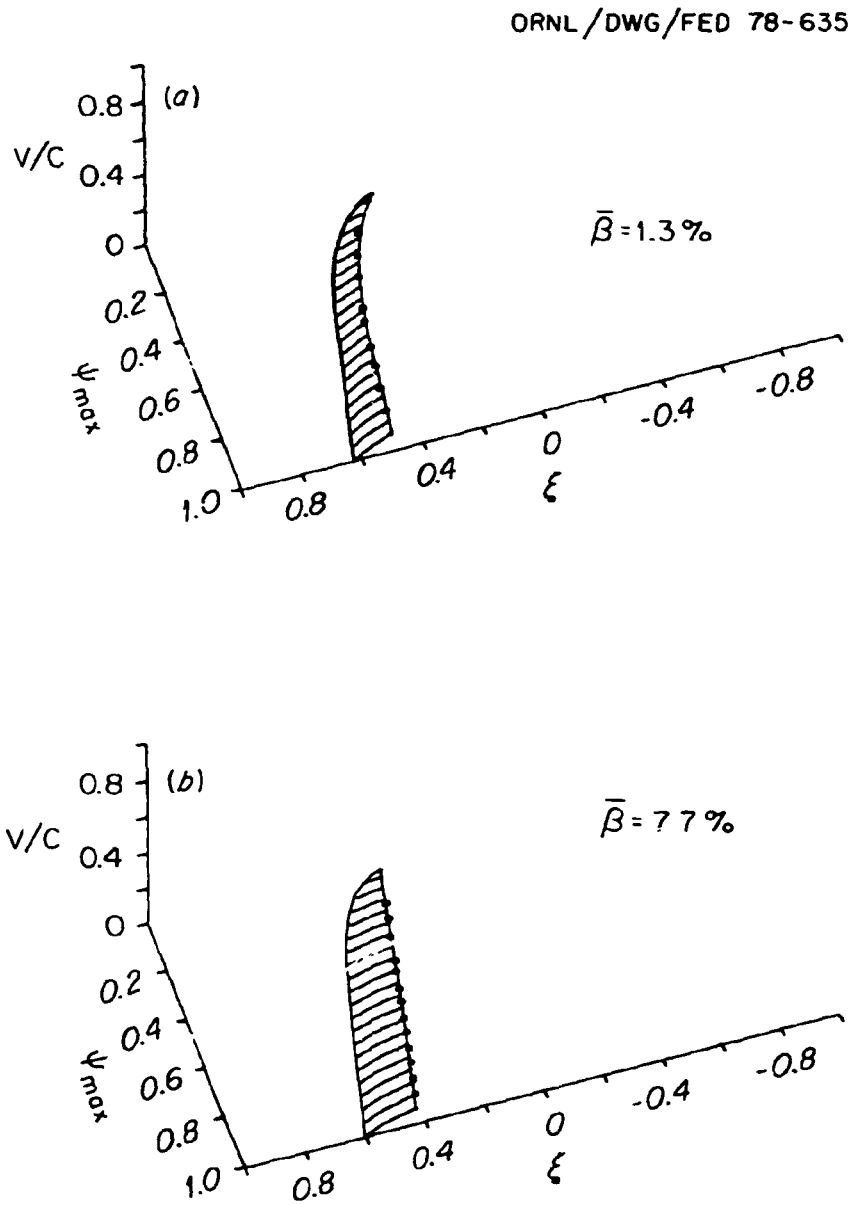

FIGURE 11. The counterpinch orbit locus. (a) β = 1.3%. (b) β = 7.7%. These surfaces lie just inside the trapping region of Fig. 6.

The boundary of the loss region will be determined by the locus of the pinch orbits with $\psi_m = 1$. Again, the locus of these orbits must be mapped by the orbit equation to the pinch point so that the loss region is determined as part of the "counter" X-type stagnation orbit locus. This last piece of topology is shown in Fig. 7. This one surface is fully equivalent to the family of curves given by Rome et al.[1] and is not restricted to a particular region of configuration space.

VIII. SUMMARY OF THE COM SPACE TOPOLOGY

All of the previously derived topological features may be shown in one diagram that displays the relationships of the various surfaces. Figure 12 shows the entire topology of the COM space for the low and high β cases. Counter circulating particles ($\zeta < 0$) are confined below surface IV. Trapped particles lie below surface II while co circulating particles lie between surfaces II and III for $\zeta > 0$. For $\zeta < 0$ in the high β case, a new class of countercirculating particles can exist above surface III. Particles on surface I are on pinch orbits, on surface II are on D orbits, and on surfaces III and IV are on stagnation orbits. The region between surfaces III and IV is the forbidden region.

A fast ion may change its type by crossing these boundaries by means of small angle collisions with the background plasma. Bold lines on surfaces III and IV are the areas through which a circulating

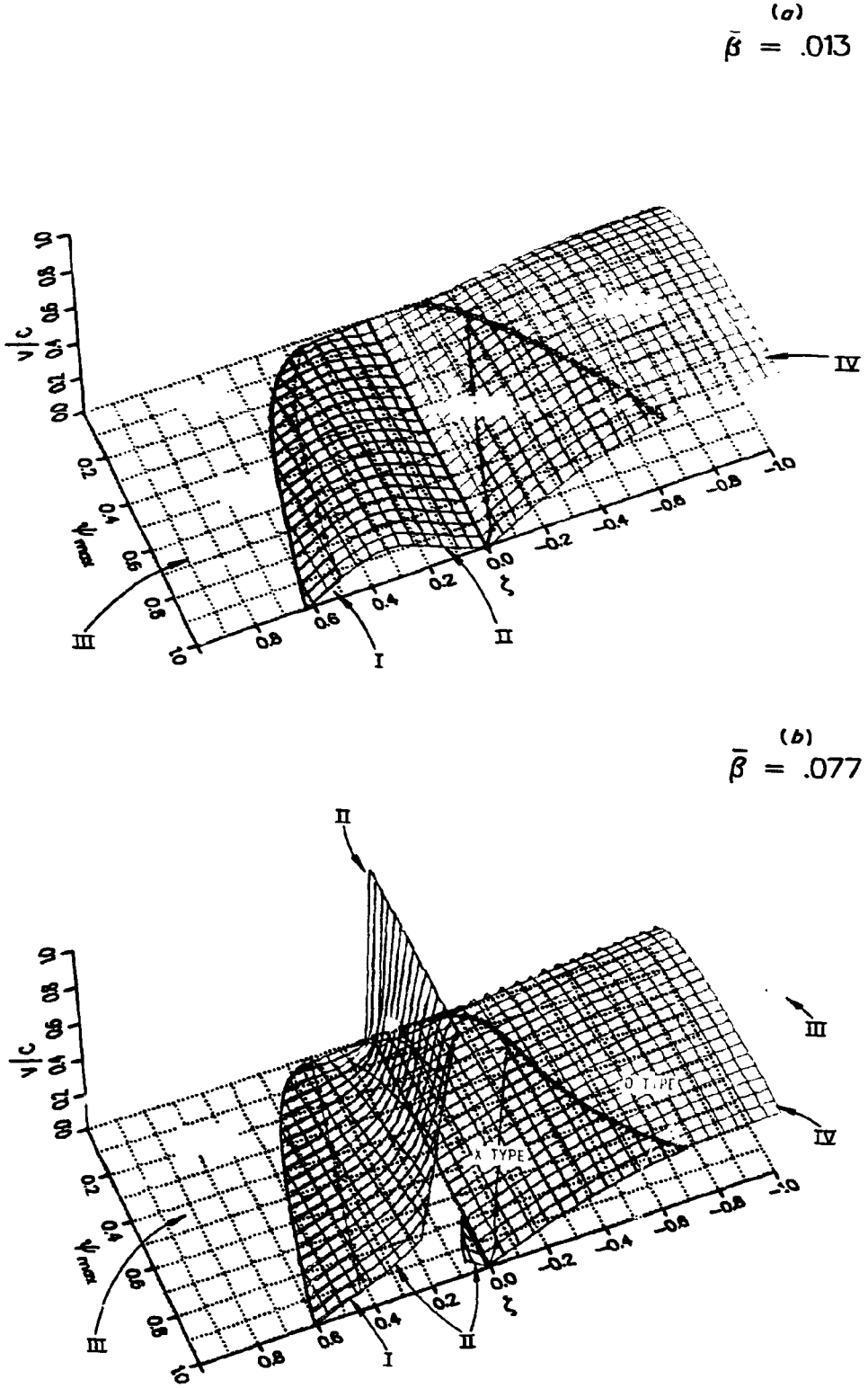

FIGURE 12. The topology of v, ζ, ψ_m space for (a) β = 1.3%. (b) β = 7.7%.

particle may enter the loss region. Transitions between the "co" and "counter" halves of the COM space can only occur by scattering through surface I.

The orbit topology in the high β equilibrium (Fig. 12b) is dramatically different from that in the low β case. First, surface II shows that high energy ($v \rightarrow c$) particles can be trapped and confined where $B'_{out}(\psi_m) > 0$ over a small range of pitch angle. Second, surface III reveals a sizeable region in which high energy cocirculating particles can be confined. Third, in the high β case, countercirculating particles may also be confined for velocities above surface III. These changes in orbit topology have resulted from the existence of minimum B in the plasma and may significantly improve energetic particle confinement in tokamaks.

Although we have plotted these pictures for alpha particles in a prototypical reactor, it is of interest to indicate what happens to the topology pictures as the particle species or the tokamak is changed. Increasing the ratio of m/e rounds off the surfaces somewhat, especially in Fig. 8b. If we made similar pictures for smaller tokamaks such as PLT or ISX, the forbidden region boundaries occur at much lower energies but go rapidly up to v/c = 1 in the high β case. Naturally, the trapping region and pinch orbit locus also appear at lower energies.

IX. DISCUSSION AND CONCLUSIONS

The COM space representation of tokamak orbits is more than a convenient way to categorize the orbits. The essential features of high energy ions that must be accounted for are their large banana widths and consequent nonlocal nature. This especially manifests itself when discussing the distribution function of the fast ions.

For example, is it meaningful to know the distribution function of the fast ions at a fixed point in space? The answer is surely no because the complicated nature of the orbit topology can cause the distribution function to change drastically for a small change in position in configuration space. As we have seen, stagnation orbits and pinch points only occur on the equatorial plane so that the fast ion density may often be strongly peaked in this region. Furthermore, for a given point in configuration space, we really have no intuition about which particular fast ion orbits will pass through the point and contribute to the distribution function there.

These difficulties are circumvented by representing the distribution function in the COM space since each individual orbit in the tokamak is fully represented therein. A distribution function in the COM space tells us immediately how many particles occupy each orbit in the tokamak and we can tell (on the average) where the particles are on those orbits so long as we are only interested in time scales long compared to a bounce time.

Of course, for applications such as injection heating, we need to know quantities such as the power delivered to a particular flux

surface by the fast ions. These quantities can be calculated from $f(v, \zeta, \psi_m)$ by means of suitable bounce averages.

COM space may also be suitable for solving the fast ion slowing down problem via the Fokker-Planck equation. So long as collisions occur infrequently compared to a bounce time, the constants of motion of each particle will change slowly. In this case, a multiple time scale expansion of the drift kinetic equation shows that

$$\frac{\partial f(v,\zeta,\psi_m)}{\partial t} = \frac{1}{\tau_b} \oint C[f(v,\zeta,\psi_m)] \frac{d\psi}{\bar{v}_D \cdot \nabla\psi} \quad , \tag{17}$$

where τ_b is the bounce time and C is the Fokker-Planck collision operator. The advantage of this approach to the slowing down problem is the physical insight that it affords and the slow time scale involved. However, the bounce averages involved are difficult and time-consuming, and the boundary conditions have been examined and found to be difficult to treat numerically.

In conclusion, we have devised a representation that fully treats the guiding center orbit topology in noncircular, high β tokamaks. The interrelationships between the various types of orbits have been clarified and formulas for calculating the topology have been given. The COM orbit representation is especially useful for treating high energy particles and some applications of this topology are presently being explored.

X. ACKNOWLEDGEMENTS

The authors wish to thank L. M. Hively for checking the logic and algebra, D. J. Strickler for providing the equilibrium data used in this paper, and R. H. Fowler for providing Fig. 3.

We have greatly benefitted from helpful discussions with D. J. Sigmar and R. Goldston. Finally, we utilized the M.I.T. symbolic manipulation computer program, MACSYMA, for much of the algebra in this paper.

REFERENCES

[1] ROME, J.A., McALEES, D.G., CALLEN, J.D., FOWLER, R.H., "Particle-orbit loss regions and their effects on neutral-injection heating in axisymmetric tokamaks," Nucl. Fusion 16 (1976) 55.

[2] HIVELY, L.M., MILEY, G.H., Fusion product bombardment of a tokamak first wall, Nucl. Fusion 17 (1978) 1031.

[3] CLARKE, J.F., SIGMAR, D.J., "Global properties of high pressure flux conserving tokamak equilibria," Phys. Rev. Lett. 38 (1977) 70.

[4] NORTHROP, T.G., ROME, J.A., "Extensions of guiding center motion to higher order," Phys. Fluids 21 (1978) 384.

[5] DORY, R.A., PENG, Y.-K.M., "High pressure flux-conserving tokamak equilibria," Nucl. Fusion 17 (1977) 21.

[6] McAlees, D.G., Alpha Particle Energetics and Neutral Beam Heating in Tokamak Plasmas, ORNL-TM/4661, Oak Ridge National Laboratory (Nov. 1974).

[7] STIX, T.H., "Heating of toroidal plasmas by neutral injection," Plasma Phys. 14 (1972) 367.